JOURNAL OF VIROLOGY, Nov. 2006, p. 10382–10394 Vol. 80, No. 21
0022-538X/06/$08.00+0 doi:10.1128/JVI.00747-06

Murine Hepatitis Virus Strain 1 Produces a Clinically Relevant Model of Severe Acute Respiratory Syndrome in A/J Mice

Nadine De Albuquerque,[1,4] Ehtesham Baig,[5] Xuezhong Ma,[1,4] Jianhua Zhang,[1,4] William He,[1,4] Andrea Rowe,[1,4] Marlena Habal,[1,4] Mingfeng Liu,[1,4] Itay Shalev,[1,4] Gregory P. Downey,[1,4] Reginald Gorczynski,[2,4] Jagdish Butany,[3] Julian Leibowitz,[7] Susan R. Weiss,[6] Ian D. McGilvray,[2,4,5] M. James Phillips,[3,4] Eleanor N. Fish,[5] and Gary A. Levy[1,4,5]*

Departments of Medicine,[1] Surgery,[2] and Pathology,[3] the Multi Organ Transplant Program,[4] University Health Network, University of Toronto,[5] Toronto, Ontario, Canada; Department of Microbiology, University of Pennsylvania, Philadelphia, Pennsylvania[6]; and Department of Microbial and Molecular Pathogenesis, Texas A&M University System-HSC, College Station, Texas[7]

Received 12 April 2006/Accepted 5 August 2006

Severe acute respiratory syndrome (SARS) is a life-threatening infectious disease which has been difficult to study and treat because of the lack of a readily available animal model. Intranasal infection of A/J mice with the coronavirus murine hepatitis virus strain 1 (MHV-1) produced pulmonary pathological features of SARS. All MHV-1-infected A/J mice developed progressive interstitial pneumonitis, including dense macrophage infiltrates, giant cells, and hyaline membranes, resulting in death of all animals. In contrast, other mouse strains developed only mild transitory disease. Infected A/J mice had significantly higher cytokine levels, particularly macrophage chemoattractant protein 1 (MCP-1/CCL-2), gamma interferon, and tumor necrosis factor alpha. Furthermore, FGL2/fibroleukin mRNA transcripts and protein and fibrin deposits were markedly increased in the lungs of infected A/J mice. These animals developed a less robust type I interferon response to MHV-1 infection than resistant C57BL/6J mice, and treatment with recombinant beta interferon improved survival. This study describes a potentially useful small animal model of human SARS, defines its pathogenesis, and suggests treatment strategies.

Severe acute respiratory syndrome (SARS) was first diagnosed in China in November 2002 and quickly spread to Hong Kong, Singapore, Vietnam, Taiwan, and Canada (15, 20, 42). SARS was documented in approximately 8,000 persons globally and resulted in over 700 deaths. Outbreaks in research laboratory personnel and the recent discovery of a new reservoir of the etiologic virus argue that further outbreaks will arise (21).

The causative agent, SARS coronavirus (SARS-CoV), best fits within group 2 coronaviruses, which include the mouse hepatitis viruses (MHV) (6, 12, 15). The clinical severity of SARS varied considerably, presumably because of the genetic diversity of the host immune response (26). Considerable variation among SARS patients with respect to circulating viral load and patterns of SARS-CoV-evoked cytokine responses have been reported, although serum levels of gamma interferon (IFN-γ), IL-10, CXCL10 (IP-10), CCL5 (RANTES), and CXCL8 (IL-8) were elevated in most patients(54). However, the underlying pathogenetic mechanisms have not been clearly elucidated.

At present, no effective therapeutic strategies have been developed for SARS. Treatments initially used during the last outbreak of SARS included ribavirin and corticosteroids (38, 46). Subsequently, hyper-immune globulin, protease inhibitors, and IFNs were considered as alternative options for treating SARS patients (57). Two groups, including our own, showed potential effectiveness for IFN in SARS (2, 27). In one study, IFN-α was shown to inhibit viral replication in vitro and to ameliorate disease in vivo. In a second study, our group demonstrated the potential efficacy of IFN-α in the treatment of SARS-infected patients (27).

Coronaviruses are known to cause a broad spectrum of diseases in animals, including pneumonia, hepatitis, nephritis, enteritis, and encephalitis. The type and severity of disease are influenced by the age and genetic background of the host, the route of infection, and the coronavirus strain (58). Members of the *Coronaviridae* family share replicative and transcriptional features. In humans, coronaviruses were thought to only cause upper respiratory infections and have only been rarely implicated in lower respiratory tract infections (33). Unlike influenza virus, human respiratory coronaviruses, other than SARS-CoV, do not cause epithelial cell necrosis. Thus, the SARS-CoV must have distinct characteristics leading to its unique pathogenicity.

MHV has served as a model for dissecting the viral and immunologic determinants of coronavirus disease (3, 28, 41, 53, 55). Extensive analysis of A59/JHM chimeric viruses has demonstrated that, while the spike gene is a major determinant of tropism and virulence in the central nervous system (39, 40), other viral genes play major roles in determining the ability to infect the liver (34) as well as the type and extent of both innate and T-cell responses induced (44). Infection of mice with recombinant viruses in which the replicase genes of JHM and A59 have been exchanged demonstrates that the presence of 3′ structural genes rather than the replicase determines the dif-

* Corresponding author. Mailing address: Toronto General Hospital, 585 University Ave., NCSB-11-1236, Toronto, Ontario M5G 2N2, Canada. Phone: (416) 340-5166. Fax: (416) 340-3378. E-mail: glfgl2@attglobal.net.

ferences in tropism and virulence between these strains (23). We have demonstrated that the macrophage prothrombinase FGL2/fibroleukin is an important determinant of disease in MHV-3-induced fulminant hepatitis and that the coronavirus nucleocapsid gene mediates much of its effect by inducing FGL2/fibroleukin (30, 36, 37). The MHV E gene is an inducer of apoptosis (1), the M gene of TGEV coronavirus is an inducer of IFN-α (22), and expression of the HE protein enhances the neurovirulence of a virus expressing the MHV-JHM spike (18). Resistance to MHV has been shown to involve both the host innate and adaptive immune systems (29, 47, 53, 56). Animals susceptible to MHV-3 generate an early increased proinflammatory response and predominant Th2 cytokine profile leading to activation of coagulation and tissue necrosis, whereas resistant animals generate a predominant TH1 immune response leading to production of cytotoxic T-lymphocyte and protective B-cell responses (4, 35, 41). In a comparison of a highly neurovirulent recombinant JHM with the weakly neurovirulent A59, the high lethality of the former is associated with an inability to induce a robust CD8T cell response (44). These studies serve as an excellent background for the study of a SARS model in mice.

None of the reported models of SARS produce lung pathology similar to that seen in humans and thus are best suited to studying the inhibitory effects of antiviral agents. In this report, we demonstrate that MHV-1 infection of inbred strains of mice produces a lethal SARS-like disease in A/J mice with features similar to those found in human patients, whereas other mouse strains including C57BL/6J mice fully recover. We further define differences in cytokine and type I IFN responses in resistant and susceptible mice and confirm a role for IFN in treatment for the viral disease.

MATERIALS AND METHODS

Mice. Female BALB/cJ, C57BL/6J A/J, and C3H/St mice 6 to 8 weeks of age (Charles River Laboratories and Jackson Laboratories) were maintained in microisolated cages and housed in the animal colony at Toronto General Hospital, University of Toronto, and fed standard lab chow diet and water ad libitum. All protocols were approved by the Animal Welfare Committee.

Virus. Parental viruses MHV-3, MHV-A59, MHV-JHM, MHV-S, and MHV-1 were obtained from the American Type Culture Collection, Manassas, VA. Viruses were first plaque purified and then expanded in murine 17CL1 cells. Supernatants were collected and subsequently stored at −80°C until used. Mice were infected with 5,000 PFU intranasally unless otherwise stated.

Cells. The origins and growth of 17Cl-1, L2, and L929 cells have been previously described (48).

Viral infection and IFN-β treatment. All viral infection studies were performed in a viral isolation room. Mice were anesthetized by intraperitoneal injection with 0.2 ml (or 10% of their body weight) 10% pentobarbital diluted in normal saline. Immediately, mice received an intranasal inoculation of 5×10^3 PFU MHV-1 in 50 μl ice-cold Dulbecco's modified Eagle's medium. The virus (5×10^3 PFU) was instilled into the nares, and mice were observed until the virus was inhaled. Mice were monitored daily for symptoms of disease, including ruffled fur, tremors, and lack of activity. Additionally, three groups of 10 A/J mice in each were infected intranasally with MHV-1 and either mock treated with phosphate-buffered saline (PBS) or treated with IFN-β: 10 mice received 10^6 IU of IFN-β 24 h prior to virus infection, 10 mice received 10^6 IU of IFN-β 12 h post-virus infection, and 10 mice received PBS at 12 h postinfection. IFN-β and PBS were administered by intraperitoneal inoculation.

Tissue isolation. Mice were sacrificed on days 0, 2, 8, 14, and 21 postinfection. Blood was collected via cardiac puncture, and serum was stored at −80°C. Liver, lung, heart, kidney, spleen, and brain were collected at the times indicated for histology, viral titers, and molecular analysis. Samples denoted for histology were fixed in 3 ml of 10% formalin. Histology samples were processed by standard methods. Samples for viral titers were snap-frozen in prelabeled cryovials in liquid nitrogen and subsequently stored at −80°C.

Viral titers. Samples were homogenized in 10% ice-cold DMEM utilizing a Polytron homogenizer (Fisher Scientific, Whitby, Ontario, Canada). Viral titers were determined in L2 cells as described previously (24).

Western blot analysis. Lung homogenates from each mouse strain were prepared for Western immunoblot analysis. Samples were processed for Western immunoblots as described previously (58). Briefly, cell lysates were resolved by sodium dodecyl sulfate-polyacrylamide gel electrophoresis, and resolved proteins were transferred to membranes and then immunoblotted with antibody to MHV-1 nucleocapsid protein and visualized using chemiluminescence. β-Actin served as a loading control.

RNA extraction and cDNA synthesis. Animal tissues snap-frozen at −80°C were thawed, and then RNA was extracted using Invitrogen TRIZOL reagent, as per the manufacturer's instructions. cDNA was synthesized using 1 μg RNA in the presence of random primers and Moloney murine leukemia virus reverse transcriptase (Invitrogen, Burlington, Ontario, Canada) according to the manufacturer's protocol.

Real-time PCR for detection of type I IFNs and FGL2. Reaction components were obtained from the LightCycler FastStart DNA Master SYBR green^{PLUS} I kit (Roche). The LightCycler instrument (Roche) and corresponding software were used for all reactions. The reaction conditions used are as follows. The PCR was performed in a final volume of 20 μl containing 1 × Master SYBR green^{PLUS} I buffer, various amounts of primer, and 5 μl of template cDNA (concentration, 100 ng/ml). The following primers and reaction conditions were used for real-time PCR: IFN-α1, 5′ ATGGCTAGGCTCTGTGCTTTCC 3′ and 5′ TCA TTTCTCTTCTCTCAGTCTTC 3′; IFN-α2, 5′ AAAGGGGAGCCTCCTCAT 3′ and 5′ TGCTTTCCTCGTGATGCTGA 3′; IFN-α4, 5′ CATGATCCTAGT AATGATGAGCTACTACT 3′ and 5′ TCAAGAGGAGGTTCCTGCATCAC 3′; IFN-α5, 5′ CAAAGCCTGTGTGATGCAA 3′ and 5′ ACTCCTGCTCAAT CTTGCCA 3′; IFN-α9, 5′ CCTCTGCTTTCCTGATGGTCT 3′ and 5′ CAGT TCCTTCATCCCG 3′; IFN-α11, 5′ CTGGCAAGATTGAGTGAAGAAGAG AAGGCT 3′ and 5′ ATAAACAAACAAATAAATAACAAATAGGTGCG 3′; IFN-α12, 5′ AGCAAAATGGAGAGAACTGTCATAGA 3′ and 5′ ATGACA TTGCTAATTACTGTT 3′; IFN-β, 5′ ACACAAGCTTAACCACCATGAACA ACAGGTGGATCCTCCACGC 3′ and 5′ GTTAGGAATTCTCAGTTTTGG AAGTTTCTGGTAAGTCTTCG 3′; Fgl2, 5′ GTCACAGCCGGTTCAAC ATCT 3′ and 5′ TGTAGGCCCCACTGCTGCTC; and hypoxanthine phosphoribosyltransferase (HPRT), 5′ CAAGCTTGCTGGTGAAAAGGA 3′ and 5′ TGAAGTACTCATTATAGTCAAGGGCATATC 3′. The annealing temperatures and primer concentrations for the various genes utilized in real-time PCR analysis are as follows: IFN-α1, 68°C and 10 pmol; IFN-α2, 65°C and 10 pmol; IFN-α4, 65°C and 10 pmol; IFN-α5, 65°C and 10 pmol; IFN-α9, 55°C and 10 pmol; IFN-α11, 45°C and 10 pmol; IFN-α12, 45°C and 10 pmol; IFN-β, 60°C and 20 pmol; Fgl2, 60°C and 10 pmol; and HPRT, 60°C and 20 pmol.

Cytokine analysis. Serum cytokine levels were assayed using cytometric bead array kits (BD Biosciences, Mississauga, Ontario, Canada): a Th1/Th2 cytokine kit which detects IL-2, IL-4, IL-5, tumor necrosis factor alpha (TNF-α), and IFN-γ and an inflammation kit which detects IL-6, IL-10, CCL2 (MCP-1), IFN-γ, TNF-α, and IL-12p70. Serum samples were processed as per the manufacturer's instructions and analyzed using a Becton Dickinson FACScan flow cytometer.

Immunohistochemistry and in situ hybridization. (i) Double-staining immunohistochemistry to detect fgl2 and fibrin. Immunohistochemical staining for detection of the fgl2 prothrombinase was used to assess fgl2 prothrombinase expression in lung tissue. Tissues were fixed with 100% methanol prior to immunostaining. A polyclonal antibody to fgl2 prothrombinase was produced in rabbits by repeated injections with a 14-amino-acid hydrophilic peptide (CKLQADDHRD-PGGN) from exon 1 of the fgl2 prothrombinase, which had been coupled to keyhole limpet hemocyanin. Antibody was purified by affinity columns, and, thereafter, tissue or cultured cell slices were incubated with antibody (20 μg/ml in PBS). For fibrin detection, a rabbit antifibrinogen antibody (DakoCytomation, Carpinteria, Calif.) was utilized. Dual staining for fgl2 and fibrin was performed using a Vecastain ABC kit (Vector Laboratories, Burlingame, Calif.) with the second antibodies labeled with alkaline phosphatase or horseradish peroxidase, respectively. Subsequently, sections were incubated with immunoperoxidase-conjugated goat immunoglobulin G (6.7 μg/ml). Sections were photographed with a Leitz Laborlux fluorescence S microscope.

(ii) Immunohistochemical staining for the infiltrating cells in lung tissue. Infiltrating cells in lung tissue from A/J mice were characterized both preinfection (day 0) and on days 2 and 8 post-MHV-1 infection by indirect immunohistochemistry using a standard avidin-biotin complex (ABC) immunoperoxidase method. A rat anti-mouse F4/80 antigen (Serotec, Raleigh, NC) at a

TABLE 1. Ability of strains of MHV to produce SARS lung pathology in BALB/cJ mice

Classical feature of SARS	Histopathology of strain[a]:				
	MHV-3	MHV-A59	MHV-1	MHV-S	MHV-JHM
Congestion	−	+	+++	−	−
Edema	−	Few foci		−	−
Hyaline membrane	−	−	+	−	−
Interstitial thickening	Limited	+	+	+	+
Interstitial inflammation	+	+	Focal	+	−
Alveolar infiltrate	+	+	+	−	−
Bronchus	Normal	Mild peribronchial inflammation	Resolving peribronchial inflammation	−	−
Pattern of disease	Pneumonitis	Focal inflammation	SARS-like (reversible)	Pneumonitis	Normal

[a] Shown is a summary of histopathological findings in BALB/cJ mice infected with different strains of MHV, including MHV-3, MHV-A59, MHV-1, MHV-S, and MHV-JHM. Scores: −, absent; +, mild; ++, moderate; +++, severe. Based on the findings, MHV-1 produces the histopathologic picture most compatible with human SARS.

1/100 dilution for detection of macrophages, a rabbit anti-human T-cell CD3 cross-reactive with mouse (Sigma, St, Louis, Mo.) at 1/400 dilution for T cells, a rat anti-mouse CD45R/B220 (BD Pharmingen, Mississauga, Ontario, Canada) at a dilution of 1/50 for B cells, and a rat anti-mouse neutrophil (Cedarlane, Mississauga, Ontario, Canada) at a dilution of 1/50 for neutrophils were used.

For morphometry, 10 high-power fields per slide were counted. Positive cells were stained positive with immunoperoxidase (brown).

In situ hybridization. The method employed for in situ hybridization has been described previously (5). A digoxigenin (DIG)-11-UTP (Roche)-labeled cDNA probe was prepared from a cloned 169-bp fragment of mfgl2 cDNA, representing nucleotides 756 (ACTGTGACA . . .) to 924 (. . . GAGTAAGGA). The DIG-UTP-labeled probe concentration was determined by immunoenzymatic reaction with chemiluminescent detection, and the probes were stored at −80°C. Tissue sections were deparaffinized in 100% xylene and 100% alcohol, followed by prehybridization in 50% formamide and 2× SSC (1× SSC is 0.15 M NaCl plus 0.015 M sodium citrate). The hybridization mixture consisted of 50% deionized formamide, 5% dextran sulfate, 250 μg of salmon sperm DNA per milliliter, and 2 μg of DIG-labeled cDNA probe per milliliter in 2× SSC. The hybridization mixture with the probe was denatured by heating in an 85°C water bath and added to tissue sections for hybridization at 42°C overnight. Hybridization was followed by application of 3% blocking reagent and incubation with polyclonal anti-DIG Fab conjugated to alkaline phosphatase. Sections were counterstained with methylene green and mounted with Permount (Fisher Scientific, Whitby, Ontario, Canada) for viewing.

Electron microscopy. (i) Transmission electron microscopy sample preparation. Electron microscopy was performed on lung samples stored at 4°C in fixative (2.5% glutaldehyde, 3.2% paraformaldehyde, 1.0 M phosphate buffer, pH 7.2). Samples were postfixed with 1% osmium tetroxide diluted in phosphate buffer, followed by en bloc staining with 2.5% uranyl acetate. Samples were then dehydrated using a graded series of ethanol and treated with propylene oxide. Epoxy resin Epon-Araldite was used as the embedding material, and sections were cut on a Riechert Ultracut E microtome and collected on 300 mesh copper grids. Samples were stained using uranyl acetate followed by Reynold's lead citrate. Grids were analyzed with a Hitachi H7000 electron microscope at 75 kV.

(ii) Immunogold electron microscopy. Tissues were fixed in 4% paraformaldehyde and 0.1% glutaraldehyde in 0.1 M phosphate buffer, pH 7.4, and then minced to 1-mm^3 cubes in phosphate buffer, infused with 2.3 M sucrose prior to freezing in liquid nitrogen. Samples were then stored at −85°C for 48 h in a solution of absolute methanol containing 0.5% uranyl acetate. The samples were warmed to −20°C and then infiltrated with Lowicryl HM20 (Marivac Services, Halifax, Nova Scotia, Canada) and embedded and polymerized in the cold with UV. Ultrathin sections were mounted on Formvar-coated nickel grids. The sections were incubated with antibody against MHV-N (nucleocapsid protein) followed by incubation with goat anti-murine immunoglobulin G–10-nm gold particle complexes (GE Healthcare, Piscataway, N.J.) and stained with uranyl acetate. The grids were examined using a JEOL JEM 1240 electron microscope (JEOL, Tokyo, Japan).

RESULTS

MHV-1 produces SARS-like pulmonary disease in BALB/cJ mice. In a first set of experiments, we examined the ability of a large number of murine coronavirus strains, including MHV-1, MHV-A59, MHV-JHM, MHV-S, and MHV-3 to produce SARS-like pathology (Table 1). BALB/cJ mice were initially studied as they are known to be highly susceptible to many MHV strains when infected by the intraperitoneal and intracerebral routes. BALB/cJ mice inoculated with 10^5 PFU of MHV-1 intranasally developed pulmonary disease with partial characteristic features of human SARS, including interstitial pulmonary infiltrates, hyaline membranes, giant cells, congestion, and hemorrhage (Fig. 1a). In addition to diffuse pulmonary infiltrates, a few focal deposits of fibrin were seen around small arterial blood vessels and in alveolar spaces with entrapment of platelets. Changes were noted as early as 2 days postinfection and progressed to day 14. Clinically these mice became lethargic with rapid respiration, but all mice survived and pulmonary pathology resolved by day 21. Livers of MHV-1-infected BALB/cJ mice sacrificed on day 8 showed portal infiltrates which by day 14 progressed to portal-portal bridging (data not shown). In contrast, BALB/cJ mice inoculated intranasally with MHV-S and MHV-JHM developed neither liver nor lung pathology. Although MHV-3 and MHV-A59 produced pulmonary lesions, these were milder than those generated by MHV-1 and did not have the characteristics of lesions described in SARS-infected patients. In addition, MHV-A59- and MHV-3-infected mice all developed severe hepatic necrosis and died of liver failure by day 10, and thus these strains of MHV do not represent relevant models of SARS. Taken together, these studies suggested that MHV-1 produced a mild SARS-like disease in BALB/cJ mice, a mild but significant liver injury, but the disease was transitory and all of the infected mice survived.

MHV-1 infection of A/J mice produces clinical and pathological SARS-like disease with high mortality. Since the C57BL/6J, C3H/St, and A/J strains have previously been shown to exhibit various degrees of susceptibility to other coronaviruses, including MHV-3 and MHV-A59, we inoculated all of these strains of mice with MHV-1 intranasally. MHV-1-infected C57BL/6J mice developed only mild pulmonary disease

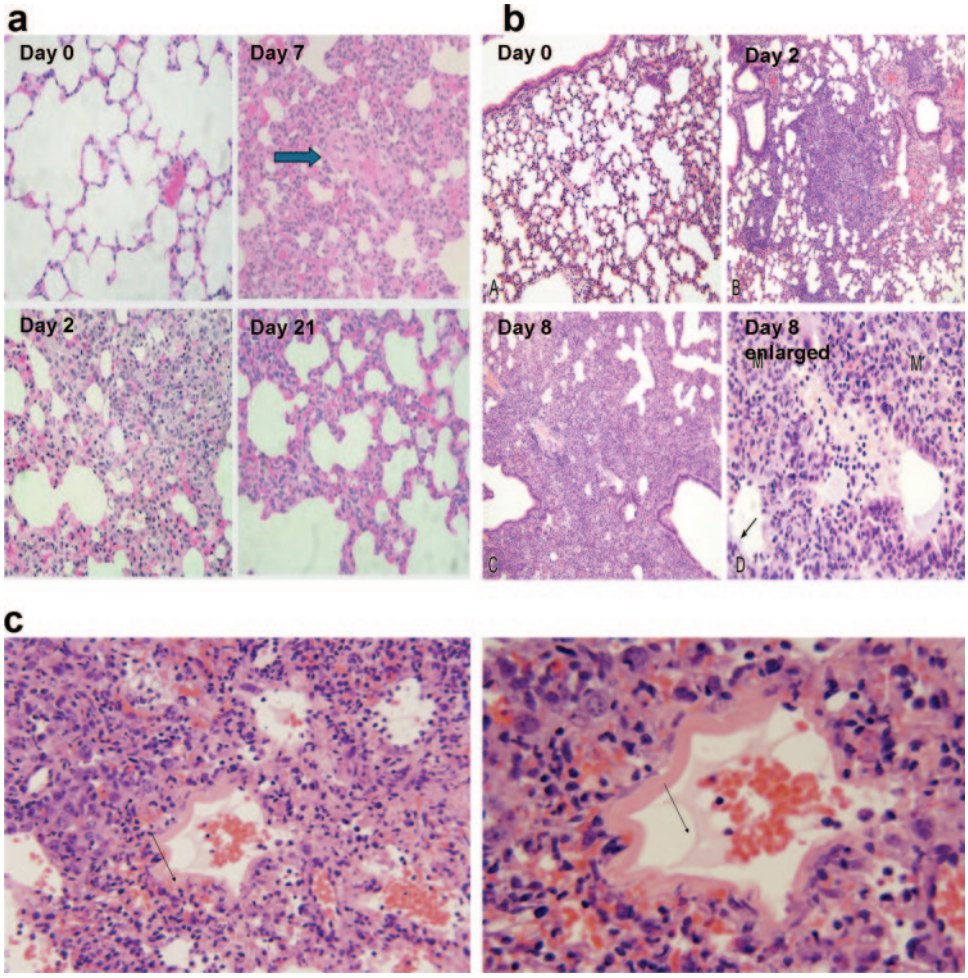

FIG. 1. Histopathology of MHV lung infection. (a) Histopathology of BALB/cJ mice infected with MHV-1 showing resolving interstitial pneumonitis. On day 2 postinfection, hemorrhage and inflammatory interstitial cell infiltrates are prominent. By day 7, hyaline membranes can be seen (arrow), and by day 21, pneumonitis is resolving (hematoxylin and eosin stain; magnification, ×200). (b) Histopathology of MHV-1-infected A/J mice. The upper left panel represents day 0 preinfection, showing normal alveoli (hematoxylin and eosin stain; magnification, ×100). The upper right panel represents 2 days post-MHV infection, showing mononuclear infiltrates with nodular formation (hematoxylin and eosin stain; magnification, ×100). The lower left panel shows severe diffuse pneumonitis with consolidation on day 8 postinfection (magnification, ×100). The lower right panel is a close-up of the lower left panel showing mononuclear cell infiltrates and hyaline membrane (arrow) (magnification, ×200). (c) MHV-1-infected A/J mice on day 8 postinfection showing details of interstitial inflammation and hyaline membranes (arrow). The right panel is a higher magnification (×500) of the left panel (×250) showing further details of hyaline membranes.

similar to that seen in BALB/cJ mice by day 2 postinfection. The pulmonary disease progressed to day 8, but by day 14 postinfection, the pulmonary lesions improved and completely resolved (data not shown).

In contrast, A/J mice developed severe progressive pulmonary disease by day 2 post-MHV-1 infection and all MHV-1-infected A/J mice died within 7 to 10 days of infection. On day 2, patchy interstitial alveolar thickening and fluid accumulation in alveolar spaces (pulmonary edema) were prominent. At death, lungs showed severe interstitial pneumonitis with large areas of complete consolidation of the lungs. The interstitial inflammatory reaction included hyaline membranes, fibrin deposition, and heavy lymphocyte and macrophage infiltrates (Fig. 1b and c). By immunohistochemistry, infiltrating cells in MHV-1-infected lung tissue from A/J mice were predominantly macrophages and neutrophils on both day 2 and day 6 post-MHV-1 infection, as determined by morphometric analysis. T cells (CD3 positive) were also increased in the infiltrates, especially by day 6 postinfection. In contrast, B cells were relatively unchanged. (Fig. 2a and b).

Examination of the livers of MHV-1-infected A/J mice showed near normal histology to day 6, but on day 7 just prior to death, there was severe hepatic congestion compatible with lung and heart failure as described in humans (data not shown).

Following infection with MHV-1, C3H/St mice showed an intermediate pattern of resistance/susceptibility and surviving C3H mice went on to develop chronic pulmonary changes including fibrosis and bronchial hyperplasia (data not shown). Thus, A/J mice are highly susceptible to MHV-1-induced pulmonary disease when the virus is delivered intranasally, C57BL/6J are relatively resistant, and C3H mice have an intermediate susceptibility.

A/J, C3H/St, BALB/cJ, and C57BL/6J mice (n = 10 per

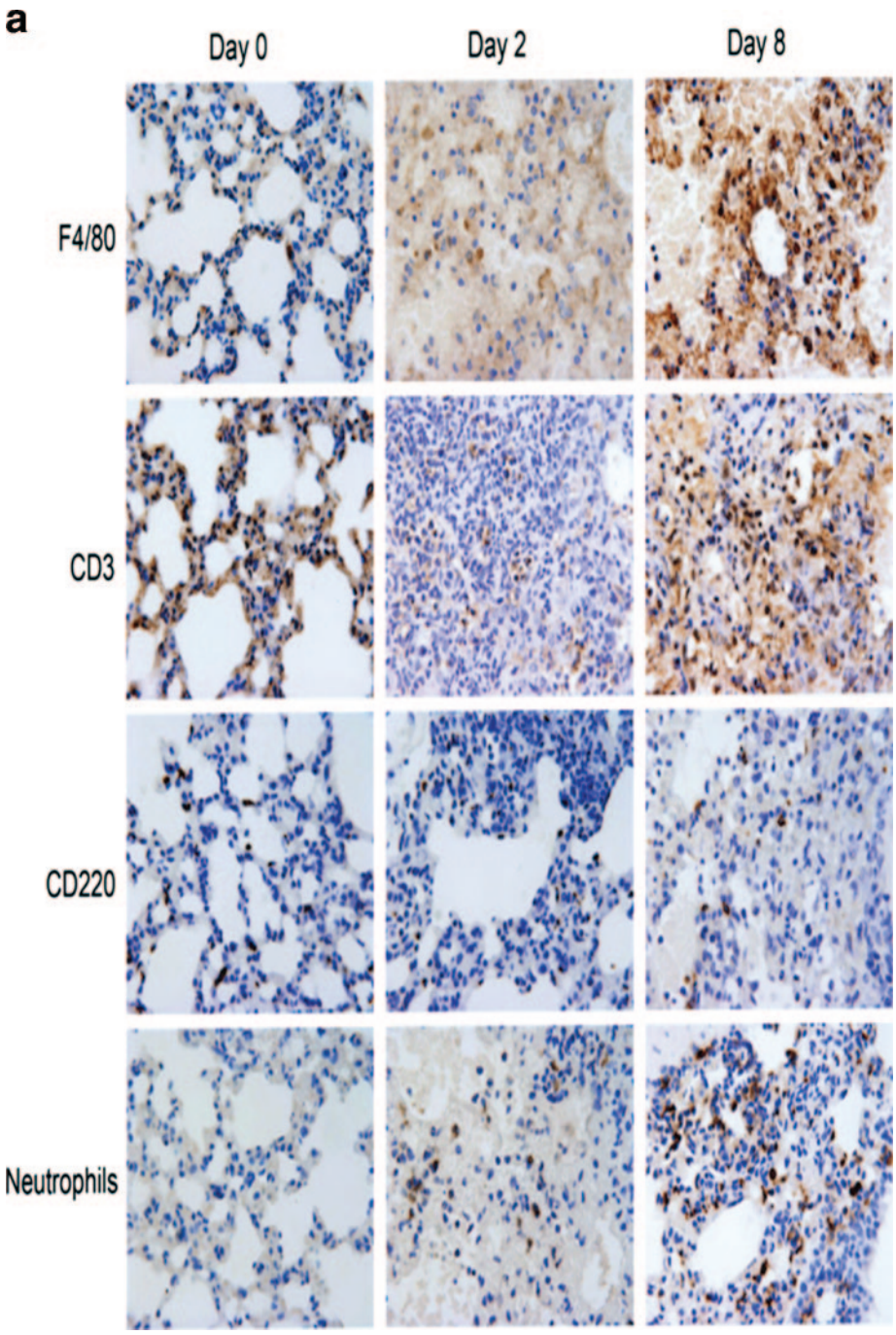

FIG. 2. (a) Immunoperoxidase stains of infiltrating cells in lung tissues from MHV-1-infected A/J mice. Columns represent days 0, 2, and 8. Rows represent different antibodies. Results are scored as follows: −, negative; +, mild positive; ++, moderate positive; +++, marked positive; ++++, most marked. (Top row) F4/80 macrophages. (Day 0) Lung showing normal tissue. Occasional resident macrophages in alveolar wall are lightly stained. No infiltrate was seen. Score, +/−. (Day 2) Lung tissue showing moderate infiltrate of macrophages. Score, ++. (Day 8) Lung with consolidated heavy infiltrate of macrophages. Score, ++++. (Second row) CD3 T cells. (Day 0) Lung showing normal tissue with mild background staining. Score, −. (Day 2) Lung with scattering of positively stained T lymphocytes. Score, +. (Day 8) Lung consolidation and numerous positive T lymphocytes. Score, +++. (Third row) CD220 B cells. Lung shows occasional positive B lymphocytes. Score, +. (Bottom row) Neutrophils. (Day 0) Lung with no positively stained cells in this micrograph. Score, −. (Day 2) Lung infiltrate with a small number of neutrophils. Score, +. (Day 8) Lung consolidation and numerous neutrophils. Score, +++. All micrographs are of immunoperoxidase-stained slides. Magnification, ×400. (b) Morphometric analysis for specific cell lineage infiltration. Data are expressed on the *y* axis as the number (mean ± standard deviation) of positive cells per high-power field (HPF). The number of days postinfection is given on the *x* axis. The lung infiltrate was a mixed-cell type with a marked increase in macrophages (F4/80), but increases in neutrophils and T cells ($CD3^+$), especially by day 8 postinfection, were observed.

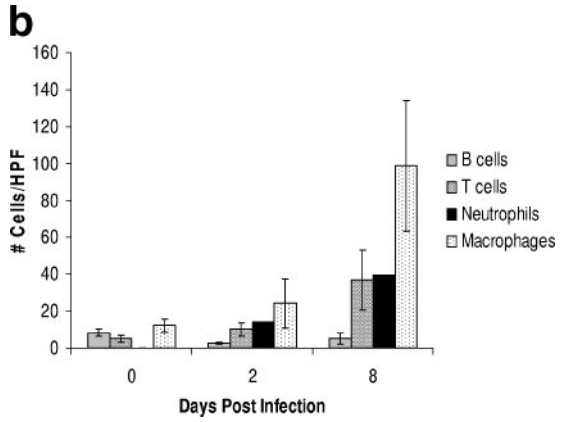

FIG. 2—*Continued.*

group) were inoculated intranasally with MHV-1 (5×10^3 PFU) and monitored closely for clinical signs of disease and survival (Fig. 3a). A/J mice, which are resistant to MHV-3 infection, developed clinical signs of disease within 48 h of intranasal inoculation of MHV-1 infection and succumbed within 8 days. In contrast, although BALB/cJ and C57BL/6J mice developed pulmonary disease, these animals cleared virus by day 14 and all mice survived. C3H mice developed an intermediate pattern of susceptibility with 40% mortality (Fig. 3a). A/J mice were then inoculated with increasing concentrations of MHV-1 (5×10^3 to 5×10^3 PFU) intranasally, and survival was monitored to day 21 (Fig. 3b). In dose-response studies, the 50% lethal dose (LD_{50}) for A/J mice infected with MHV-1 was calculated to equal 2.4×10^2 PFU using the method of Reed and Muench (43).

Expression of FGL2/fibroleukin is associated with pulmonary fibrin deposits. Fibrin deposition is a prominent feature of SARS (7, 16). Our previous studies of coronavirus-induced fulminant hepatitis demonstrated that cell surface expression of the immune coagulant fgl2/fibroleukin led to organ-damaging microvascular thrombosis (25, 30). We therefore examined lung tissue from both susceptible A/J mice and resistant C57BL/6J mice infected with MHV-1 for the presence of FGL2 mRNA transcripts, protein, and fibrin (Fig. 4). As shown in Fig. 4a, fgl2 protein was expressed by inflammatory cells and type 1 pneumocytes in juxtaposition to deposits of fibrin. Furthermore, by in situ hybridization, FGL2 transcripts were detected in the cytoplasm of terminal alveoli and respiratory bronchioles (Fig. 4b). Also of interest, the bronchial epithelial cells are fused, forming giant cells, a hallmark of human SARS (Fig. 4b). Lungs from BALB/cJ and C57BL/6 mice had neither FGL2 nor fibrin deposits. Real-time reverse transcriptase PCR (RT-PCR) quantification of FGL2 transcripts demonstrated increased FGL2 mRNA expression in the lungs of A/J mice at 2 and 4 days postinfection, whereas FGL2 mRNA expression decreased in C57BL/6J mice post-MHV-1 infection (Fig. 4c).

Virus localization and viral burden in MHV-1-infected mice. A detailed examination of the lungs was made using transmission electron microscopy and immunogold electron microscopy on MHV-1 lung samples. On day 1 postinfection, virions were identified in the peripheral airways adjacent to capillaries in the alveolar walls (Fig. 5, left panel). A cluster of virions is seen at the arrow. The same particles are seen at higher magnification in the panel on the right. The virus particles occurred singly or in clusters. Individual particles were easily recognized by their uniform size and electron density. This result is important because it confirms that the virions reached the distal airways. There is also evidence of reaction to the viruses by the greatly enhanced vesicular activity noted in the capillary shown; it reflects the transport of fluid across the cell, which is greatly enhanced. It is a manifestation of edema formation,

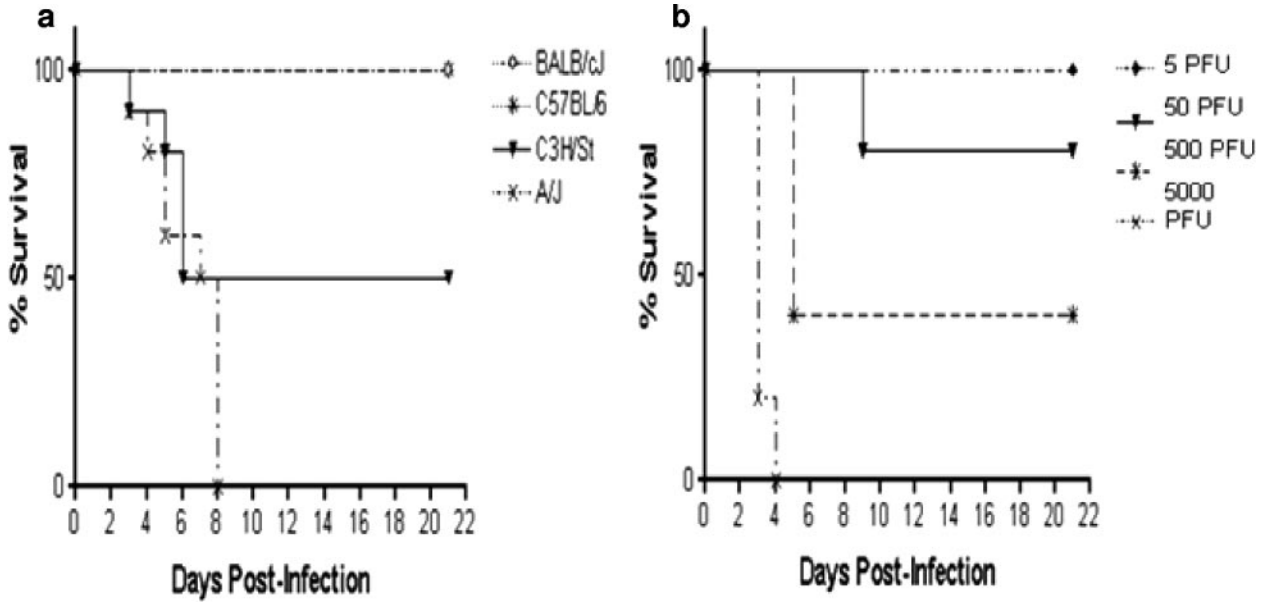

FIG. 3. Effect of MHV-1 on survival of inbred strains of mice. (a) Effect of MHV-1 infection on survival of BALB/c, C57BL/6J, A/J, and C3H/ST mice ($n = 10$ per group). Panel b shows the effect of increasing doses of MHV-1 on survival of A/J mice. Data were used to determine the LD_{50} by the method of Reed and Muench (43).

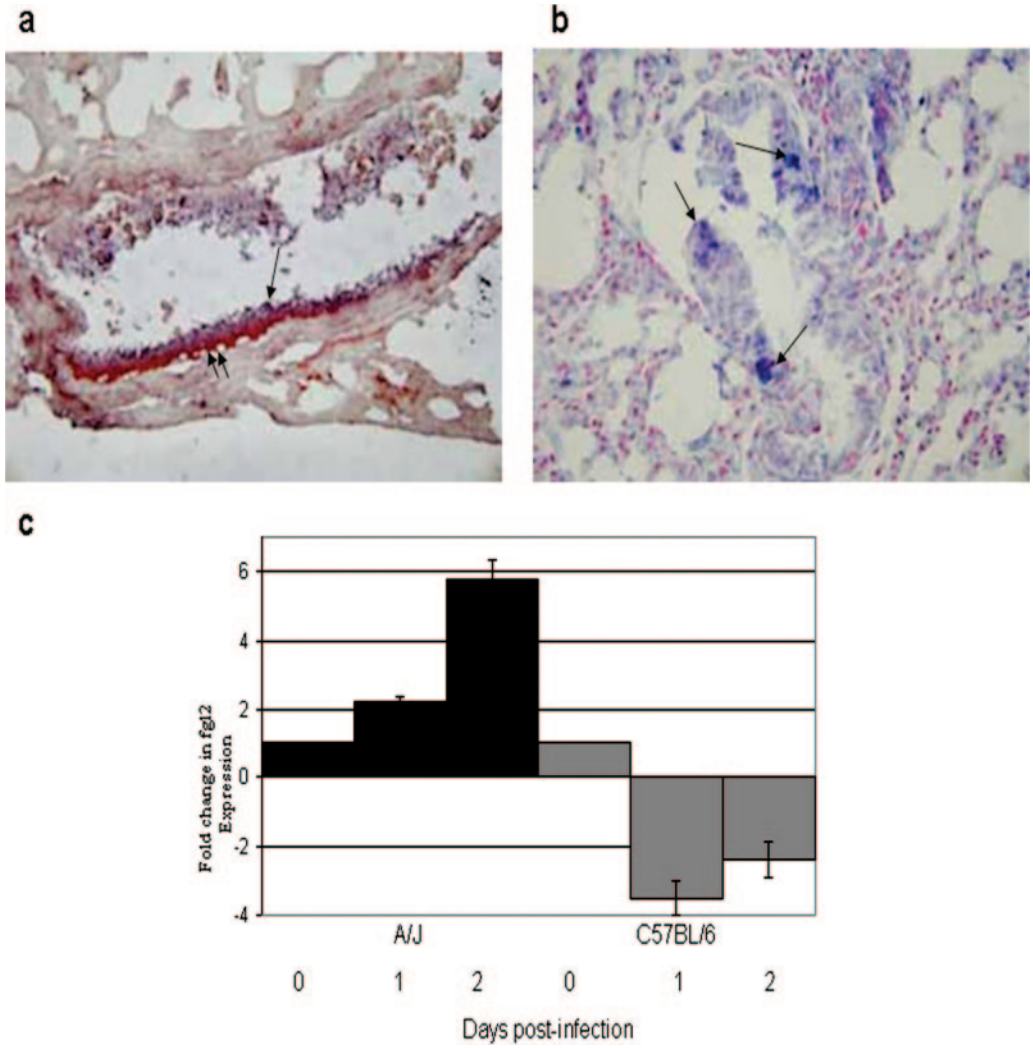

FIG. 4. Localization of fibrinogen-like protein (fgl2) and fibrin by immunohistochemistry and in situ hybridization in lung tissues from MHV-1-infected A/J mice 2 days postinfection. (a) By immunohistochemistry, bronchial epithelium is positive for fgl2 protein (blue staining, single arrow); dense fibrin deposits are seen along the wall of the bronchial (red staining, double arrow) (magnification, ×400). (b) FGL2 mRNA transcripts are seen in bronchial lining cells (blue staining, single arrow); many are fused, forming giant cells (magnification, ×400). (c) The increased number of FGL2 mRNA transcripts in lung of MHV-1-infected A/J mice was determined by real-time PCR. In contrast, no increase in FGL2 mRNA transcripts was seen in lung in C57BL/6J mice. Data represent the mean ± standard deviation of three independent experiments done in triplicate.

which is an early reaction to the presence of the virus. Note also the neutrophil in the capillary lumen. By day 4, there was a notable infiltrate as seen also by light microscopy with lymphocytes, neutrophils, and macrophages. Electron microscopy showed extensive alveolar wall damage with fibrin, cell fragments, free red blood cells, virions, inflammatory cells, lymphocytes, macrophages, and neutrophils (not shown). By day 8, the lung was consolidated; the electron microscopic examination confirmed the predominance of macrophages, which often occurred in sheets and were the predominant cells in the infiltrate. Many cell fragments and red blood cells were also seen; alveolar walls were largely destroyed. A striking finding was that the macrophages were filled with viral particles. Measurement of the particles using the electron microscope point-to-point measurement software confirmed the correct measurement of the particles as expected for coronavirus virions. To further confirm that they were indeed coronaviruses, immunoelectron microscopy was done, which confirmed their presence, their size, and their occurrence within macrophages. Note the presence of gold-labeled antibodies localized to the particles within macrophages. This is a very heavy infection of viruses; each macrophage is filled with virions. (Fig. 5)

Viral burden in lung, brain, spleen, and liver from both C57BL/6J and A/J mice was determined, using a standard plaque assay, as described previously (24). Virus was first detected in the lungs of A/J mice at 12 h postinfection, reached maximal levels by 48 to 72 h, and persisted at high levels until death of the animals on day 7 postinfection (Fig. 6a, left panel). Although virus was also recovered from the brain, liver, and spleen of MHV-1-infected A/J mice, it was detected later in the course of disease and at 4- to 5-log-fold-lower levels than

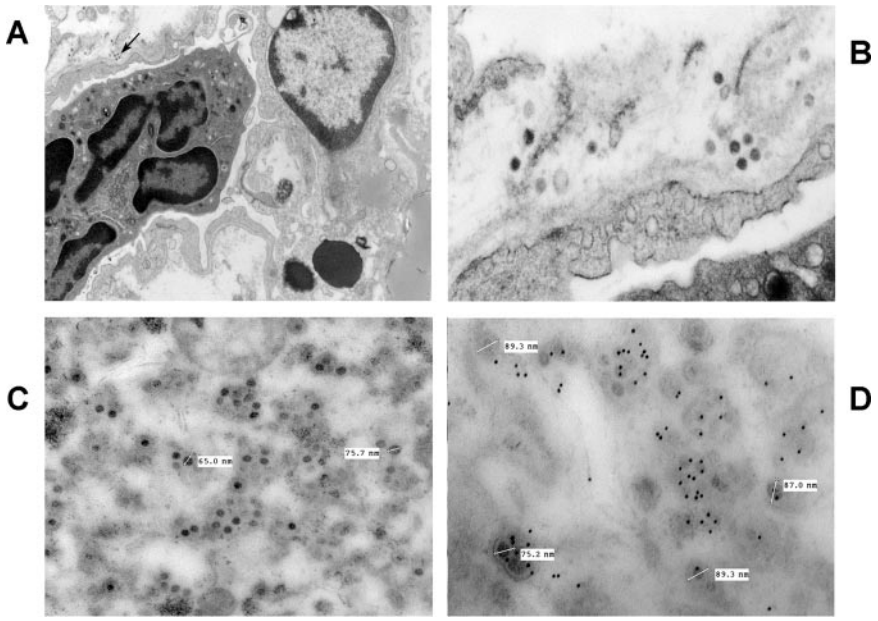

FIG. 5. Transmission electron microscopy (TEM [A to C]) and immunoelectron microscopy (IEM [D]) detection of virions in A/J lung tissues. (A) Virions (indicated by the arrow) are detectable in peripheral pulmonary airways; they are located outside the capillary wall of the lung on day 1. Viral particles are in close proximity to the plasma membrane of an endothelial cell within the alveolar wall. A neutrophil (darkly staining cell) is observed within the blood vessel. (B) Higher magnification of panel A. Virions are adjacent to endothelial cell basement membranes. In addition, vesicles are apparent in large numbers in endothelial cells of alveolar capillaries. By TEM (C), the small dense particles are virions are packed into lysosomes within a macrophage. Virion size (as indicated, ranging from 65 to 90 nm in diameter) corresponds to MHV. By IEM (D), 10-nm gold particles conjugated to anti-MHV nucleocapsid antibody are localized within pulmonary macrophages, confirming the viral nature of the particles. Virion diameters are 65 to 90 nm, typical of coronaviruses.

that seen in lung tissue (Fig. 6a, left panel). Virus was also detected in the lungs of disease-resistant C57BL/6J mice by 12 h postinfection, but at a lower titer than in A/J mice (Fig. 6A, right panel). Maximal levels of virus were reached by day 4, but no virus was detected by day 7 to 10 postinfection.

Lung tissues were examined for the presence of nucleocapsid protein by Western immunoblotting (Fig. 6b). In lung tissue from A/J mice, nucleocapsid protein was detected as early as 12 h postinfection and persisted to time of death of the animals on day 8 postinfection. Nucleocapsid protein was also detected in the lungs of C57BL/6J and BALB/cJ mice by day 2 postinfection and was detected even at 21 days postinfection at a time when infectious virus was undetectable by plaque assay.

Immune response to MHV-1: proinflammatory cytokine levels correlate with disease activity. In subsequent time course experiments, we examined the cytokine expression profiles in sera from MHV-1-infected A/J and C57BL/6 mice. Serum was collected from A/J and C57BL/6J mice both prior to MHV-1 infection and at various times postinfection and analyzed for IL-10, IL-6, IL-12p70, IFN-γ, TNF-α, and macrophage chemoattractant protein 1 (MCP-1/CCL2) (Fig. 6c). Notably, we observed marked elevation of IL-6, IL-10, IFN-γ, TNF-α, and CCL2 expression in infected A/J mice compared with infected C57BL/6 mice. In a separate set of experiments, sequential measurements of serum levels of TNF-α and IFN-γ were undertaken in both resistant and susceptible mice (Fig. 6d). At all time points postinfection, levels of both cytokines were higher in susceptible A/J mice. Levels of TNF-α peaked on day 6 postinfection, whereas levels of IFN-γ were highest at 2 days postinfection. These results parallel observations in SARS patients.

IFN response and protective effects of IFN-β in MHV-1-infected A/J mice. To investigate the IFN response in the differentially susceptible strains, lung tissues from MHV-1-infected C57BL/6J and A/J mice were examined for gene expression for different IFN-α subtypes and IFN-β. Notably, levels of IFN induction, as measured by gene expression, were significantly lower in A/J than in the C57BL/6J mice (Fig. 7a). Transcriptional activation of the early response IFNs, IFN-β, and IFN-α4 was evident by 12 h postinfection, whereas gene expression for IFN-α1, IFN-α2, and IFN-α5 reached maximal levels at 24 h postinfection and then returned to basal levels by day 7 postinfection. No virus-inducible gene induction for IFN-α9, IFN-α11, or IFN-α12 was detectable in either mouse strain challenged with MHV-1.

Given our observation that A/J mice exhibited lower levels of type I IFN expression in the lung, we next examined the effect of administering exogenous IFN-β on A/J survival in response to MHV-1 infection. In this experiment, A/J mice were infected and either left untreated or treated with IFN-β. Two different IFN treatment regimens were employed: a single dose of 10^6 U/mouse at 24 h prior to virus infection or a single dose of 10^6 U/mouse 12 h post-virus challenge. As expected, the mice in the untreated group all succumbed to MHV-1 infection by day 5 postinfection with MHV-1 (Fig. 7b). Mice that received IFN-β 12 h post-virus inoculation exhibited an increased survival time, but all eventually succumbed to disease. Mice that were treated with IFN-β 24 h prior to viral

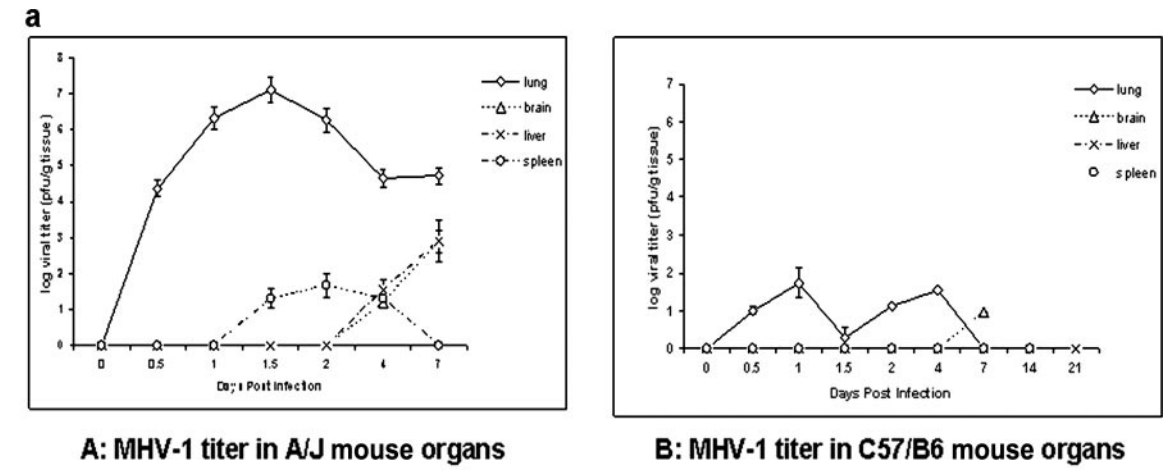

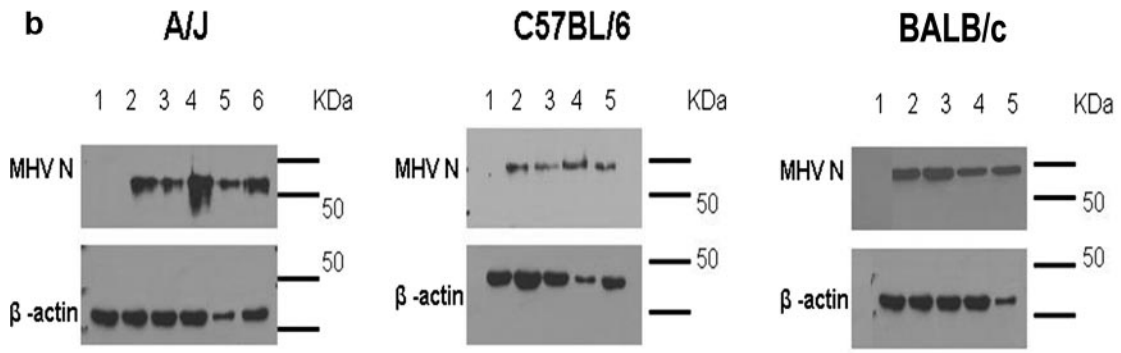

c

	day 0 p.i.		day 6 p.i.	
cytokine	A/J	C57BL/6	A/J	C57BL/6
IL-10	26.7±3	24.6±4	164±22	38±12
IL-6	53.8±4.9	48.6±5	546±23	215±20
IL-12p70	306±30.6	298±29	642.5±36	449.3±21
IFN-γ	14.7±1.4	13.9±2	555±62	236±34
TNF-α	25.2±2.5	18±2	163±22	68±12
MCP-1	166±16	159±16	7400±400	225±40

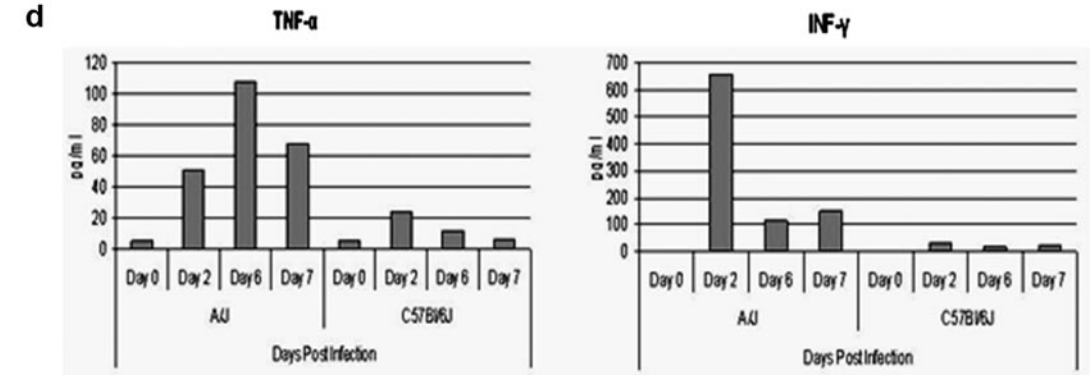

FIG. 6. Viral titers in tissues and cytokine responses. (a) Viral titers from lung (◇), brain (△), liver (×), and spleen (○) from MHV-1-infected A/J mice and C57BL/6 mice at various times postinfection. (b) Western immunoblot detection of nucleocapsid protein in lungs. A/J mice: lane 1, day 0; lane 2, 12 h postinfection; lane 3, 24 h postinfection; lane 4, 4 days postinfection; lane 5, 6 days postinfection; and lane 6, 8 days postinfection.

challenge showed delayed onset of disease and an increased survival rate.

DISCUSSION

Although a number of models for SARS have been proposed, including SARS-CoV infection of mice (49), SARS-CoV infection of cats and ferrets (31), and SARS-CoV infection of nonhuman primates (13, 32), none of the models produce lung pathology or mortality similar to that seen in humans. Thus, these models can be utilized at best for evaluating the effectiveness of agents, including neutralizing antibodies, putative vaccines, or antiviral agents on viral replication. As reported herein, the MHV-1 mouse model produces a SARS-like clinical and pathological syndrome in which pathogenic mechanisms can be dissected.

MHV-1 was first isolated in Mill Hill, United Kingdom, and was reported to cause fatal hepatitis in the inbred P strain mice (10). Even in early studies, the pathogenicity of the virus was variable and critically dependent upon a number of immune-modulating variables, including coinfection with enterococci (11), Friend virus, or Moloney virus (9), and neurotropic and pneumotropic MHV-1 variants have been described (50, 52). Similarly, host age plays an important role in susceptibility to the virus; C57BL/6J, C3H, P, and Swiss Webster strains of mice have been noted to be very susceptible to intraperitoneal MHV-1 in the first 2 weeks of life, but susceptibility decreases as they age (10, 51, 52).

In the present study, we found that intranasal infection with MHV-1 produces a strain-dependent disease. The A/J mice, known to be resistant to the lethality of MHV-A59 and MHV-3 infection, all died following intranasal infection with MHV-1. Although BALB/cJ and C57BL/6J mice developed pulmonary disease, these animals cleared the virus by day 14 and survived. C3H mice developed an intermediate pattern of susceptibility with 40% mortality. The cell infiltrates seen in MHV-1-infected A/J mice were predominantly macrophages, with modest numbers of $CD3^+$ T cells and neutrophils similar to that seen in human SARS (16). Peak viral titers were 10^4-fold higher in susceptible A/J mice in comparison to resistant C57BL/6J mice, an observation confirmed by lung tissue electron microscopy in which more virions were present in A/J than C57BL/6J and BALB/cJ lung tissue cells. Interestingly, virions were seen largely in pulmonary macrophages rather than epithelial cells, consistent with our previous observations in MHV-3-induced fulminant hepatitis. These findings argue that host factors are critically important for the development of SARS-like disease and suggest that, as for other coronavirus diseases, innate immune cells are an important reservoir for infection. The finding that pulmonary fgl2/fibroleukin is strongly expressed in susceptible animals, but not in resistant ones, as discussed below, is also consistent with a role for the innate immune system in acute disease.

Serum cytokines and chemokines were markedly elevated in susceptible A/J mice in comparison to those in resistant animals following MHV-1 infection. These findings are consistent with other respiratory diseases. For example, the role of proinflammatory cytokines in respiratory infections and acute respiratory distress syndrome has been previously documented (19, 45). Elevated levels of chemokines including CCL2 and CCL3 are seen in respiratory syncytial virus infections. Equally, elevations in IL-1β, TNF-α, IFN-γ, and IL-12 have been reported in mice infected with human adenovirus (17). Patients with acute respiratory distress syndrome (ARDS) also have marked elevations in TNF-α and IL-6 (45). These elevated cytokines and chemokines may contribute to the immunopathology of SARS. Recently we and others have reported that serum concentrations of IFN-γ, IL-10, CXCL10, CCL5, and CXCL8 were elevated in SARS patients, especially in those patients with a poor outcome. In SARS patients, expression levels of IL-10, IFN-γ, and CXCL10 peaked within 4 days of peak viral titers, whereas IL-12p70, IL-4, and TNF-α were highest 5 to 7 days after peak viral loads. Similarly, during MHV-1 infection of A/J mice, high levels of IFN-γ and TNF-α were seen after peak viral titers were observed. The fact that corticosteroids ameliorated disease in some SARS patients is consistent with the hypothesis that an immunopathological mechanism may underlie the lung damage associated with SARS (54) as it is known that corticosteroids inhibit formation of proinflammatory cytokines. Furthermore, it has been reported that lower levels of both IL-6 and TNF-α are associated with better responses to steroid treatment in ARDS (14, 54).

We previously reported that MHV-3 induces FGL2, an inflammatory immune coagulant, which results in fibrin deposition and hepatic necrosis (24, 30). In the MHV-1 model of SARS, both FGL2 mRNA transcripts and fgl2 protein were also seen in close association with deposits of fibrin in diseased lungs from A/J mice, suggesting that this inflammatory mediator may be contributing to the pathogenesis of SARS as well. Previously we reported that the nucleocapsid protein from strains of virus that caused massive hepatic necrosis, including MHV-3 and MHV-A59, induced transcription of FGL2. At present, we have no information whether the N gene from MHV-1 similarly induces FGL2 transcription. More recently, we have reported that IFN-γ can induce macrophage production of FGL2 and that, although TNF-α alone cannot induce FGL2 transcription, it synergizes with IFN-γ, leading to a marked enhancement in FGL2 transcription and subsequent thrombosis (8, 24, 30). In view of the findings of marked elevations of IFN-γ and TNF-α, both in the MHV-1-induced

BALB/cJ mice: lane 1, uninfected control; lane 2, 2 days postinfection; lane 3, 8 days postinfection; lane 4, 14 days postinfection; lane 5, 21 days postinfection. C57BL/6 mice: lane 1, uninfected control; lane 2, 2 days postinfection; lane 3, 8 days postinfection; lane 4, 14 days postinfection; lane 5, 21 days postinfection. Nucleocapsid protein was detected as a 50-kDa band. Measurement of β-actin levels was performed to ensure equal loading of protein. (c) Determination of inflammatory cytokines from uninfected and MHV-1-infected A/J and C57BL/6 lungs on day 0 or 6 postinfection. (d) Sequential measurements of serum levels of TNF-α and IFN-γ were undertaken in both resistant and susceptible mice. At all time points postinfection, levels of both cytokines were higher in susceptible A/J mice. Levels of TNF-α peaked on day 6 postinfection, whereas levels of IFN-γ were highest at 2 days postinfection.

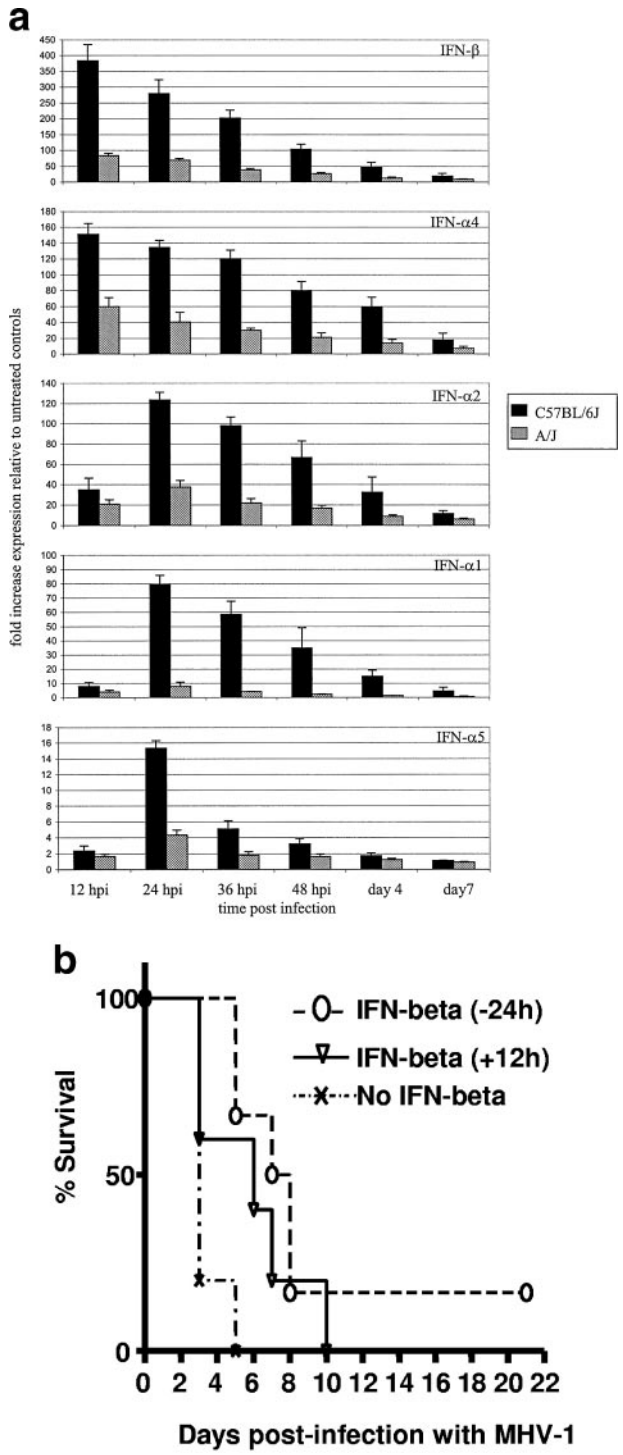

FIG. 7. Levels of type I interferon correlate with resistance to MHV-1. (a) Mice were infected intranasally with 10^5 PFU of MHV-1, and at at each of the time points indicated, five mice were euthanized, their lung tissue was harvested, the RNA was extracted, and the cDNA was synthesized, as described in Materials and Methods. For each sample, reference (HPRT) and target (IFN-α1, IFN-α2, IFN-α4, IFN-α5, IFN-α9, IFN-α11, IFN-α12, and IFN-β) quantitative RT-PCRs were performed. The data are presented as the change (fold) in expression relative to an untreated control sample ± standard error. (b) A/J mice ($n = 10$ per group) were (i) treated with 10^6 IU of IFN-β 24 h prior to intranasal infection with 10^5 PFU of MHV-1 (○) or 12 h postinfection (inverted triangle) or (ii) treated with PBS at 12 h postinfection (×). Mice were monitored for survival once daily.

experimental model and in patients with SARS-CoV infection, this could have relevance to disease pathogenesis.

Based on the observation that intranasal infection with MHV-1 results in a dramatically more aggressive disease in A/J mice versus C57BL/6J mice, we examined whether the type and extent of the lung IFN response to infection might shape the outcome. A/J mice displayed significantly lower levels of type I IFN gene induction compared with C57BL/6J mice. Gene induction for IFN-α9, IFN-α11, and IFN-α12 was absent in response to MHV-1 in both mouse strains. The kinetics of gene induction, namely early expression of IFN-β and IFN-α4 and later gene expression of IFN-α1, IFN-α2, and IFN-α5, agree with the sequential phosphorylation and activation of IRF3 followed induction and activation of IRF7. We next examined the effect of IFN-β treatment on the course of viral disease in A/J mice. The data revealed protective effects of IFN-β treatment. Mice that received IFN-β 24 h prior to virus infection exhibited a delayed onset of disease and increased survival. At the end of the study, mortality had decreased from 100 to 80% and 50% survival was extended from 3 to 8 days. Mice that received IFN-β 12 h post-virus infection also exhibited a delayed onset of disease, but survival was unaffected. The potential benefit of IFN treatment for respiratory coronavirus infections was reported in patients treated with IFN alfacon-1 during the recent SARS outbreak in Toronto. IFN alfacon-1-treated SARS patients displayed a more rapid recovery than patients treated with corticosteroids, in terms of time taken to resolve lung abnormalities, their oxygen saturation, their requirement for supplemental oxygen, and resolution of clinical measurements indicative of disease severity: lactate dehydrogenase and creatine kinase levels (29).

Although it is unclear whether SARS will continue to be a major human health problem, the isolation of SARS-CoV from Himalayan palm civets and bats suggests that an animal reservoir for SARS-CoV continues to exist (21). Furthermore, bat feces is used in traditional Chinese herbal medicines for treatment of asthma and kidney ailments and general malaise and additionally bat meat is a delicacy. Therefore, it is quite possible that additional SARS outbreaks will occur.

Thus, this model offers the potential to provide further insights into the pathogenesis of coronavirus-induced lung injury and the contribution of both the virus and host immune response. Furthermore, the data that we have generated in our animal model has great relevance to the pathogenesis of human SARS and support a role for IFN treatment as an effective therapy.

ACKNOWLEDGMENTS

This work was supported by grants from the Canadian Institute for Health Research (grants MOP 1504, 2003H00308, and 37780); the Ontario Research and Development Challenge Fund; and grants AI51493, AI62817, and AI17418 from the National Institutes of Health.

REFERENCES

1. **An, S., C.-J. Chen, X. Yu, J. L. Leibowitz, and S. Makino.** 1999. Induction of apoptosis in murine coronavirus-infected cultured cells and demonstration of E protein as an apoptosis inducer. J. Virol. **73:**7853–7859.
2. **Cinatl, J., B. Morgenstern, G. Bauer, P. Chandra, H. Rabenau, and H. W. Doerr.** 2003. Treatment of SARS with human interferons. Lancet **362:**293–294.
3. **Dindzans, V. J., P. J. MacPhee, L. S. Fung, J. L. Leibowitz, and G. A. Levy.**

1985. The immune response to mouse hepatitis virus: Expression of monocyte procoagulant activity and plasminogen activator during infection in vivo. J. Immunol. **135:**4189–4197.
4. **Dindzans, V. J., B. Zimmerman, A. Sherker, and G. A. Levy.** 1987. Susceptibility to mouse hepatitis virus strain 3 in BALB/cJ mice: failure of immune cell proliferation and interleukin 2 production. Adv. Exp. Med. Biol. **218:** 411–420.
5. **Ding, J. W., Q. Ning, M. F. Liu, A. Lai, K. Peltekian, L. Fung, C. Holloway, H. Yeger, M. J. Phillips, and G. A. Levy.** 1998. Expression of the fgl2 and its protein product (prothrombinase) in tissues during murine hepatitis virus strain-3 (MHV-3) infection. Adv. Exp. Med. Biol. **440:**609–618.
6. **Drosten, C., S. Gunther, W. Preiser, S. Van Der Werf, H. R. Brodt, S. Becker, H. Rabenau, M. Panning, L. Kolesnikova, R. A. Fouchier, A. Berger, A. M. Burguiere, J. Cinatl, M. Eickmann, N. Escriou, K. Grywna, S. Kramme, J. C. Manuguerra, S. Muller, V. Rickerts, M. Sturmer, S. Vieth, H. D. Klenk, A. D. Osterhaus, H. Schmitz, and H. W. Doerr.** 2003. Identification of a novel coronavirus in patients with severe acute respiratory syndrome. N. Engl. J. Med. **348:**1967–1976.
7. **Farcas, G. A., S. M. Poutanen, T. Mazzulli, B. M. Willey, J. Butany, S. L. Asa, P. Faure, P. Akhavan, D. E. Low, and K. C. Kain.** 2005. Fatal severe acute respiratory syndrome is associated with multiorgan involvement by coronavirus. J. Infect. Dis. **191:**193–197.
8. **Ghanekar, A., M. Mendicino, H. Liu, W. He, M. Liu, R. Zhong, M. J. Phillips, G. A. Levy, and D. R. Grant.** 2004. Endothelial induction of fgl2 contributes to thrombosis during acute vascular xenograft rejection. J. Immunol. **172:**5693–5701.
9. **Gledhill, A. W.** 1961. Enhancement of the pathogenicity of mouse hepatitis virus (MHVI) by prior infection of mice with certain leukaemia agents. Br. J. Cancer **15:**531–538.
10. **Gledhill, A. W., C. H. Andrewes, and G. W. Dick.** 1952. Production of hepatitis in mice by the combined action of two filterable agents. Lancet **ii:**509–511.
11. **Gledhill, A. W., and G. W. Dick.** 1955. The nature of mouse hepatitis virus infection in weanling mice. J. Pathol. Bacteriol. **69:**311–320.
12. **Gorbalenya, A. E., E. J. Snijder, and W. J. M. Spaan.** 2004. Severe acute respiratory syndrome coronavirus phylogeny: toward consensus. J. Virol. **78:**7863–7866.
13. **He, C., W. Pang, X. Yong, H. Zhu, M. Lei, and Q. Duan.** 2005. Experimental infection of macaques with the human reovirus BYD1 strain: an animal model for the study of the severe acute respiratory syndrome. DNA Cell Biol. **24:**491–495.
14. **Headley, A. S., E. Tolley, and G. U. Meduri.** 1997. Infections and the inflammatory response in acute respiratory distress syndrome. Chest **111:**1306–1321.
15. **Holmes, K. V.** 2003. SARS-associated coronavirus. N. Engl. J. Med. **348:** 1948–1951.
16. **Hwang, D. M., D. W. Chamberlain, S. M. Poutanen, D. E. Low, S. L. Asa, and J. Butany.** 2005. Pulmonary pathology of severe acute respiratory syndrome in Toronto. Mod. Pathol. **18:**1–10.
17. **Kajon, A. E., A. P. Gigliotti, and K. S. Harrod.** 2003. Acute inflammatory response and remodeling of airway epithelium after subspecies B1 human adenovirus infection of the mouse lower respiratory tract. J. Med. Virol. **71:**233–244.
18. **Kazi, L., A. Lissenberg, R. Watson, R. J. de Groot, and S. R. Weiss.** 2005. Expression of hemagglutinin esterase protein from recombinant mouse hepatitis virus enhances neurovirulence. J. Virol. **79:**15064–15073.
19. **Krishnan, S., M. Craven, R. C. Welliver, N. Ahmad, and M. Halonen.** 2003. Differences in participation of innate and adaptive immunity to respiratory syncytial virus in adults and neonates. J. Infect. Dis. **188:**433–439.
20. **Ksiazek, T. G., D. Erdman, C. S. Goldsmith, S. R. Zaki, T. Peret, S. Emery, S. Tong, C. Urbani, J. A. Comer, W. Lim, P. E. Rollin, S. F. Dowell, A. E. Ling, C. D. Humphrey, W. J. Shieh, J. Guarner, C. D. Paddock, P. Rota, B. Fields, J. DeRisi, J. Y. Yang, N. Cox, J. M. Hughes, J. W. LeDuc, W. J. Bellini, and L. J. Anderson.** 2003. A novel coronavirus associated with severe acute respiratory syndrome. N. Engl. J. Med. **348:**1953–1966.
21. **Lau, S. K., P. C. Woo, K. S. Li, Y. Huang, H. W. Tsoi, B. H. Wong, S. S. Wong, S. Y. Leung, K. H. Chan, and K. Y. Yuen.** 2005. Severe acute respiratory syndrome coronavirus-like virus in Chinese horseshoe bats. Proc. Natl. Acad. Sci. USA **102:**14040–14045.
22. **Laude, H., J. Gelfi, L. Lavenant, and B. Charley.** 1992. Single amino acid changes in the viral glycoprotein M affect induction of alpha interferon by the coronavirus transmissible gastroenteritis virus. J. Virol. **66:**743–749.
23. **Lavi, E., E. M. Murray, S. Makino, S. A. Stohlman, M. M. Lai, and S. R. Weiss.** 1990. Determinants of coronavirus MHV pathogenesis are localized to 3′ portions of the genome as determined by ribonucleic acid-ribonucleic acid recombination. Lab. Investig. **62:**570–578.
24. **Levy, G. A., J. L. Leibowitz, and T. S. Edgington.** 1981. Induction of monocyte procoagulant activity by murine hepatitis virus type 3 parallels disease susceptibility in mice. J. Exp. Med. **154:**1150–1163.
25. **Li, C., L. S. Fung, S. Chung, A. Crow, N. Myers-Mason, M. J. Phillips, J. L. Leibowitz, E. Cole, C. A. Ottaway, and G. A. Levy.** 1992. Monoclonal antiprothrombinase (3D4.3) prevents mortality from murine hepatitis virus infection (MHV-3). J. Exp. Med. **176:**689–697.
26. **Lin, M., H. K. Tseng, J. A. Trejaut, H. L. Lee, J. H. Loo, C. C. Chu, P. J. Chen, Y. W. Su, K. H. Lim, Z. U. Tsai, R. Y. Lin, R. S. Lin, and C. H. Huang.** 2003. Association of HLA class I with severe acute respiratory syndrome coronavirus infection. BMC Med. Genet. **4:**9. [Online.] doi:10.1186/1471-2350-4-9.
27. **Loutfy, M. R., L. M. Blatt, K. A. Siminovitch, S. Ward, B. Wolff, H. Lho, D. H. Pham, H. Deif, E. A. LaMere, M. Chang, K. C. Kain, G. A. Farcas, P. Ferguson, M. Latchford, G. Levy, J. W. Dennis, E. K. Lai, and E. N. Fish.** 2003. Interferon alfacon-1 plus corticosteroids in severe acute respiratory syndrome: a preliminary study. JAMA **290:**3222–3228.
28. **Lucchiari, M. A., J. P. Martin, M. Modolell, and C. A. Pereira.** 1991. Acquired immunity of A/J mice to mouse hepatitis virus 3 infection: dependence on interferon-gamma synthesis and macrophage sensitivity to interferon-gamma. J. Gen. Virol. **72:**1317–1322.
29. **Lucchiari, M. A., M. Modolell, R. C. Vassao, and C. A. Pereira.** 1993. TNF alpha, IL-1 and O_2^- release by macrophages do not correlate with the anti-mouse hepatitis virus 3 effect induced by interferon gamma. Microb. Pathog. **15:**447–454.
30. **Marsden, P. A., Q. Ning, L. S. Fung, X. Luo, Y. Chen, M. Mendicino, A. Ghanekar, J. A. Scott, T. Miller, C. W. Chan, M. W. Chan, W. He, R. M. Gorczynski, D. R. Grant, D. A. Clark, M. J. Phillips, and G. A. Levy.** 2003. The Fgl2/fibroleukin prothrombinase contributes to immunologically mediated thrombosis in experimental and human viral hepatitis. J. Clin. Investig. **112:**58–66.
31. **Martina, B. E., B. L. Haagmans, T. Kuiken, R. A. Fouchier, G. F. Rimmelzwaan, A. G. Van, J. S. Peiris, W. Lim, and A. D. Osterhaus.** 2003. Virology: SARS virus infection of cats and ferrets. Nature **425:**915.
32. **McAuliffe, J., L. Vogel, A. Roberts, G. Fahle, S. Fischer, W. J. Shieh, E. Butler, S. Zaki, M. St. Claire, B. Murphy, and K. Subbarao.** 2004. Replication of SARS coronavirus administered into the respiratory tract of African Green, rhesus and cynomolgus monkeys. Virology **330:**8–15.
33. **McIntosh, K., R. K. Chao, H. E. Krause, R. Wasil, H. E. Mocega, and M. A. Mufson.** 1974. Coronavirus infection in acute lower respiratory tract disease of infants. J. Infect. Dis. **130:**502–507.
34. **Navas, S., and S. R. Weiss.** 2003. Murine coronavirus-induced hepatitis: JHM genetic background eliminates A59 spike-determined hepatotropism. J. Virol. **77:**4972–4978.
35. **Ning, Q., L. Berger, X. Luo, W. Yan, F. Gong, J. Dennis, and G. Levy.** 2003. STAT1 and STAT3 alpha/beta splice form activation predicts host responses in mouse hepatitis virus type 3 infection. J. Med. Virol. **69:**306–312.
36. **Ning, Q., S. Lakatoo, M. Liu, W. Yang, Z. Wang, M. J. Phillips, and G. A. Levy.** 2003. Induction of prothrombinase fgl2 by the nucleocapsid protein of virulent mouse hepatitis virus is dependent on host hepatic nuclear factor-4 alpha. J. Biol. Chem. **278:**15541–15549.
37. **Ning, Q., M. Liu, P. Kongkham, M. M. Lai, P. A. Marsden, J. Tseng, B. Pereira, M. Belyavskyi, J. Leibowitz, M. J. Phillips, and G. Levy.** 1999. The nucleocapsid protein of murine hepatitis virus type 3 induces transcription of the novel fgl2 prothrombinase gene. J. Biol. Chem. **274:**9930–9936.
38. **Oba, Y.** 2003. The use of corticosteroids in SARS. N. Engl. J. Med. **348:** 2034–2035.
39. **Phillips, J. J., M. Chua, S. H. Seo, and S. R. Weiss.** 2001. Multiple regions of the murine coronavirus spike glycoprotein influence neurovirulence. J. Neurovirol. **7:**421–431.
40. **Phillips, J. J., M. M. Chua, G. F. Rall, and S. R. Weiss.** 2002. Murine coronavirus spike glycoprotein mediates degree of viral spread, inflammation, and virus-induced immunopathology in the central nervous system. Virology **301:**109–120.
41. **Pope, M., S. W. Chung, T. Mossmann, J. L. Leibowitz, R. M. Gorczynski, and G. A. Levy.** 1996. Resistance of naive mice to murine hepatitis virus strain 3 (MHV-3) requires development of a TH1, but not TH2 response, whereas pre-existing antibody protects against primary infection. J. Immunol. **156:**3342–3349.
42. **Poutanen, S. M., D. E. Low, B. Henry, S. Finkelstein, D. Rose, K. Green, R. Tellier, R. Draker, D. Adachi, M. Ayers, A. K. Chan, D. M. Skowronski, I. Salit, A. E. Simor, A. S. Slutsky, P. W. Doyle, M. Krajden, M. Petric, R. C. Brunham, and A. J. McGeer.** 2003. Identification of severe acute respiratory syndrome in Canada. N. Engl. J. Med. **348:**1995–2005.
43. **Reed, L. J., and H. Muench.** 1938. A simple method of estimating fifty percent points. Am. J. Hyg. **27:**493–497.
44. **Rempel, J. D., S. J. Murray, J. Meisner, and M. J. Buchmeier.** 2004. Differential regulation of innate and adaptive immune responses in viral encephalitis. Virology **318:**381–389.
45. **Samuel, C. E.** 2001. Antiviral actions of interferons. Clin. Microbiol. Rev. **14:**778–809.
46. **So, L. K., A. C. Lau, L. Y. Yam, T. M. Cheung, E. Poon, R. W. Yung, and K. Y. Yuen.** 2003. Development of a standard treatment protocol for severe acute respiratory syndrome. Lancet **361:**1615–1617.
47. **Stohlman, S. A., and L. P. Weiner.** 1981. Chronic central nervous system demyelination in mice after JHM virus infection. Neurology **31:**38–44.

48. **Sturman, L. S., and K. K. Takemoto.** 1972. Enhanced growth of a murine coronavirus in transformed mouse cells. Infect. Immun. **6:**501–507.
49. **Subbarao, K., J. McAuliffe, L. Vogel, G. Fahle, S. Fischer, K. Tatti, M. Packard, W.-J. Shieh, S. Zaki, and B. Murphy.** 2004. Prior infection and passive transfer of neutralizing antibody prevent replication of severe acute respiratory syndrome coronavirus in the respiratory tract of mice. J. Virol. **78:**3572–3577.
50. **Taguchi, F., N. Hirano, Y. Kiuchi, and K. Fujiwara.** 1976. Difference in response to mouse hepatitis virus among susceptible mouse strains. Jpn. J. Microbiol. **20:**293–302.
51. **Taguchi, F., and S. G. Siddell.** 1985. Difference in sensitivity to interferon among mouse hepatitis viruses with high and low virulence for mice. Virology **147:**41–48.
52. **Taguchi, F., R. Yamaguchi, S. Makino, and K. Fujiwara.** 1981. Correlation between growth potential of mouse hepatitis viruses in macrophages and their virulence for mice. Infect. Immun. **34:**1059–1061.
53. **Tardieu, M., C. Hery, and J. M. Dupuy.** 1980. Neonatal susceptibility to MHV3 infection in mice. II. Role of natural effector marrow cells in transfer of resistance. J. Immunol. **124:**418–423.
54. **Ward, S. E., M. R. Loutfy, L. M. Blatt, K. A. Siminovitch, J. Chen, A. Hinek, B. Wolff, D. H. Pham, H. Deif, E. A. LaMere, K. C. Kain, G. A. Farcas, P. Ferguson, M. Latchford, G. Levy, L. Fung, J. W. Dennis, E. K. Lai, and E. N. Fish.** 2005. Dynamic changes in clinical features and cytokine/chemokine responses in SARS patients treated with interferon alfacon-1 plus corticosteroids. Antivir. Ther. **10:**263–275.
55. **Williamson, J. S., K. C. Sykes, and S. A. Stohlman.** 1991. Characterization of brain-infiltrating mononuclear cells during infection with mouse hepatitis virus strain JHM. J. Neuroimmunol. **32:**199–207.
56. **Williamson, J. S. P., and, S. A. Stohlman.** 1990. Effective clearance of mouse hepatitis virus from the central nervous system requires both $CD4^+$ and $CD8^+$ T cells. J. Virol. **64:**4589–4592.
57. **Wu, W., J. Wang, P. Liu, W. Chen, S. Yin, S. Jiang, L. Yan, J. Zhan, X. Chen, J. Li, Z. Huang, and H. Huang.** 2003. A hospital outbreak of severe acute respiratory syndrome in Guangzhou, China. Chin. Med. J. (Engl. Ed.) **116:** 811–818.
58. **Yuwaraj, S., J. Ding, M. Liu, P. A. Marsden, and G. A. Levy.** 2001. Genomic characterization, localization, and functional expression of FGL2, the human gene encoding fibroleukin: a novel human procoagulant. Genomics **71:**330–338.